FEATURE ARTICLE

Resonance Raman Intensity Analysis of Vibrational and Solvent Reorganization in Photoinduced Charge Transfer

Anne Myers Kelley

Department of Chemistry, Kansas State University, Willard Hall, Manhattan, Kansas 66506-3701

Received: May 7, 1999

Quantitative analysis of resonance Raman scattering cross sections, together with charge-transfer absorption and emission spectra, can provide detailed information about the changes in nuclear equilibrium geometry undergone by both the electron donor and acceptor and the surrounding solvent in photoinduced charge-transfer processes. The molecular parameters that determine absorption and fluorescence band shapes and resonance Raman cross sections are summarized, and methods for extracting those parameters through spectral modeling are reviewed with emphasis on charge-transfer systems. Applications to the determination of molecular and solvent reorganization parameters to several organic intra- and intermolecular charge-transfer transitions are then presented, and prospects for further development of the technique are discussed.

Introduction

Electron transfer or charge transfer processes are a class of chemical reactions in which the reactants and products are distinguished primarily in differing by one (or occasionally more) units of effective charge, without any making or breaking of chemical bonds.[1] (While physicists often treat electron transfer and hole transfer on the same footing, chemists are more likely to think of all such processes as electron transfer because the electrons are the real particles with high mobility; the positive charges are attached to the nuclei and do not move from reactant to product in reactions normally classified as charge transfer.) Although the nominal bonding arrangement of the atoms is preserved, the change in charge distribution is generally accompanied by substantial changes in the equilibrium nuclear geometry of both the electron donor and acceptor and the surrounding solvent, particularly if the solvent is a highly polar liquid.[1] Since electronic transitions are assumed to be very fast compared with nuclear motions, the nuclei immediately following electron transfer find themselves in a geometry far from equilibrium, and the energy released as the nuclei relax to the equilibrium geometry of the products is referred to as the reorganization energy, traditionally symbolized λ. In many inorganic systems, such as those involving oxidation and reduction of transition-metal ions, the internal molecular ("inner-sphere") geometry change is minimal and the reorganization is overwhelmingly dominated by the solvent ("outer-sphere") contribution. In organic systems, while the solvent reorganization energy may still be large, the electron transfer is more likely to involve bonding and/or antibonding molecular orbitals of the donor and acceptor and the internal vibrational reorganization is also significant.

While many electron transfer reactions are purely thermally activated, some very important classes of electron transfer processes—those involved in photography, electrophotography, photosynthesis, and artificial solar energy conversion, to name a few—are photoinduced. Photoinduced processes may further be divided into two groups: those in which light absorption creates an electronically excited donor or acceptor which subsequently reduces or oxidizes its partner, and those in which light absorption produces the charge-separated state directly. The latter case is characterized by the appearance of a new charge-transfer absorption and/or fluorescence band not present in the donor or acceptor alone. The electronic ground and excited states of the charge-transfer transition are then also the reactants and products in the electron-transfer reaction; that is, electronic excitation corresponds to formal electron transfer from a ground-state DA to an excited-state $D^{\bullet+}/A^{\bullet-}$ (Figure 1).

The quantitative determination of the various contributions to the reorganization energy, particularly for these direct charge-transfer transitions, is of interest for two basic reasons. First, it allows us to test and extend our understanding of the electronic structure of molecular ions, the relationship between electronic structure and geometry, the vibrational dynamics of molecules, the dynamics and energetics of solvation, etc. Second, the rates of electron-transfer reactions are sensitive to the reorganization parameters.[2,3] In many cases, the decay of the ion pair state formed by direct charge-transfer excitation is dominated by radiationless transitions corresponding to formal return electron transfer, a process whose rate is described by a golden rule expression usually written as the product of a purely electronic factor and a vibrational Franck−Condon factor.[2,4−8] The vibrational part depends on the frequencies and geometry changes along all of the coupled vibrations and in fact has exactly the same form as the vibrational part of the fluorescence line shape extrapolated to zero frequency.[9−11] Thus, it can, in principle, be extracted by careful fitting of the fluorescence spectrum, but since charge-transfer fluorescence is usually vibrationally unstructured, it provides no clue as to the vibrational modes involved. Resonance Raman intensity analysis[12−15] provides, in principle, a way to obtain the complete vibrational part of the return electron-transfer problem.[9,16−18] Knowledge of these parameters should be helpful in determining how to manipulate molecular structures or solvent environments

10.1021/jp991530o CCC: $18.00
Published on Web 08/13/1999

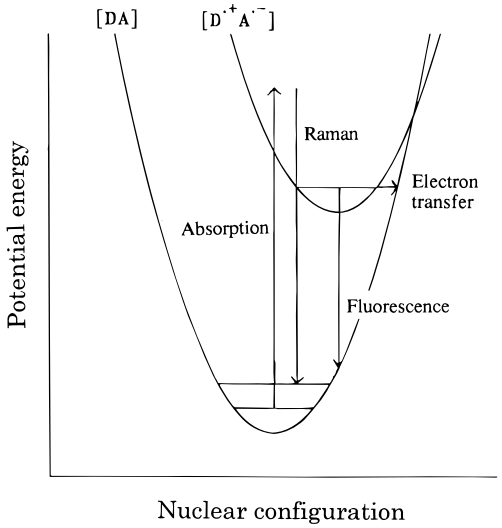

Figure 1. Schematic representation of neutral (ground) and ion pair (excited) state potential energy surfaces for photoinduced electron transfer and the relationship among the processes of optical absorption, resonance Raman, fluorescence, and nonradiative electron transfer.

to enhance or minimize particular electron-transfer pathways and/or to understand natural or artificial systems in which this has already been accomplished.[19−22]

Theory

The absorption cross section as a function of incident frequency ω for transitions between a particular pair of initial and final molecular electronic states, in the Born−Oppenheimer and Condon approximations, can be written as[23]

$$\sigma_A(\omega) = \frac{4\pi^2(eM)^2\omega}{3\hbar c}\sum_i P_i \sum_v \frac{1}{\pi}\frac{(\gamma/2)|\langle v|i\rangle|^2}{(\omega+\omega_i-\omega_0-\omega_v)^2+(\gamma/2)^2} \quad (1)$$

Here, (eM) is the electronic transition dipole moment assumed to be independent of nuclear coordinates, $|i\rangle$ and $|v\rangle$ are vibrational levels of the ground and excited electronic states, respectively, having vibrational frequencies above the zero point of ω_i and ω_v , respectively, P_i is the Boltzmann population of initial state $|i\rangle$, ω_0 is the electronic zero−zero energy, and γ is the inverse lifetime of the excited state, here assumed independent of vibrational state. For a polyatomic molecule with N atoms, each vibrational overlap is $(3N - 6)$-dimensional, although these are often approximated as products of one-dimensional overlaps. Equation 1 describes a superposition of Lorentzian vibronic transitions, each having a line width of γ, a center frequency of $\omega_0 + \omega_i - \omega_v$, and a relative intensity of $|\langle v|i\rangle|^2$, the vibrational Franck−Condon factor. If the ground and excited electronic states have nearly the same equilibrium geometries and force constants, then the Franck−Condon factor is significantly different from zero only for $|i\rangle = |v\rangle$; that is, only the zero−zero transition has significant intensity. If the ground- and excited-state potentials do have very different equilibrium geometries or frequencies along one or more vibrational normal modes, then the Franck−Condon factors for transitions involving changes of one or more quanta in those modes can be large. Since the reorganization energy simply depends on the frequency of the mode and the change in equilibrium geometry between ground and excited potentials along that mode,[1,16] analysis of a vibrationally resolved absorption spectrum gives, in principle, the frequencies and reorganization energies of all the participating vibrations.

In practice, however, it is rarely possible to obtain the requisite vibrational resolution in experimental absorption spectra of charge-transfer transitions for a combination of reasons. The absorption spectrum may be highly congested (consist of a very dense forest of lines) due to many thermally populated initial states $|i\rangle$ and a very large number of Franck−Condon active transitions arising from each initial state. When the charge-transfer molecule of interest is embedded in a liquid or solid medium, usually the "vibrational" degrees of freedom of the medium are also strongly reorganized, generating an essentially continuous distribution of Franck−Condon active modes. Furthermore, different molecules generally sit in slightly different local environments within the medium, leading to inhomogeneous broadening of the absorption spectrum which manifests itself mainly as a statistical distribution of zero−zero frequencies. The latter two effects, which are not always clearly distinguishable, have the effect of clothing each $|i\rangle \rightarrow |v\rangle$ transition of the molecule with a line shape that is orders of magnitude broader than the lifetime-limited line width γ and typically obscures most or all of the vibrational structure from the absorption spectrum. Alternative methods are needed to tease out the vibrational Franck−Condon structure that underlies the apparently diffuse spectrum. One particularly powerful such method is resonance Raman intensity analysis.[14,15]

In a Raman process, the total scattered power $P_{i\rightarrow f}$ (photons s^{-1}) arising from a particular initial to final vibrational state transition, integrated over the Raman line width and over all polarization and propagation directions for the scattered light, is given by

$$P_{i\rightarrow f} = I_L N_i \sigma_{R,i\rightarrow f} \quad (2)$$

where I_L is the laser intensity (photons s^{-1} cm^{-2}), N_i is the number of molecules in state $|i\rangle$ within the illuminated volume, and $\sigma_{R,i\rightarrow f}$ is the Raman cross section (cm^2 $molecule^{-1}$). Most experimental geometries actually detect scattering into a range of solid angles Ω about a particular direction, which is proportional to the differential cross section, $(d\sigma/d\Omega)_{R,i\rightarrow f}$. The relationship between σ and $(d\sigma/d\Omega)$ depends on the scattering geometry and the Raman depolarization ratio.[24] The usual formulation of vibrational Raman scattering assumes an isolated molecule interacting with weakly perturbing incident monochromatic radiation. The molecule starts in a vibrational state of the ground electronic surface, $|i\rangle$, and time-dependent perturbation theory is used to calculate the rate of change, in the steady-state limit, of the probability for finding the molecule in a different vibrational state $|f\rangle$ following one interaction with the incident field and one with the scattered field. The perturbed wave function resulting from each radiation−matter interaction is expanded in the stationary eigenfunctions of the molecular Hamiltonian, resulting in a summation over paths involving all intermediate states that are transition dipole coupled to both the initial and the final state. When the excitation is resonant with vibrational levels of a single, strongly allowed electronic state, it is usually assumed that only those levels contribute significantly as intermediate states, and the cross section becomes[25]

$$\sigma_{R,i\rightarrow f}(\omega_L) = \frac{8\pi(eM)^4\omega_L{\omega_S}^3}{9\hbar^2c^4}\sum_i P_i\left|\sum_v \frac{\langle f|v\rangle\langle v|i\rangle}{\omega_L+\omega_i-\omega_0-\omega_v+i\gamma/2}\right|^2 \quad (3)$$

Here ω_L and ω_S are the incident (laser) and scattered photon frequencies and the other symbols are as defined following eq 1. For the fundamentals or overtones of a particular normal mode to have intensity in the resonance Raman, there must be some intermediate state(s) $|v\rangle$ that have good overlaps with both $|i\rangle$ and $|f\rangle$, which can occur only if the potential surface for the resonant state has a different frequency and/or potential minimum from that of the ground state along that coordinate. This is the same requirement for the Franck−Condon factors $|\langle v|i\rangle|^2$ to be nonzero for $v \neq i$, and thus for that mode's frequency to appear in a vibrationally resolved absorption spectrum. However, the Raman spectrum is usually vibrationally well resolved even if the electronic spectrum is not; as discussed further below, the factors that broaden the electronic spectrum affect only the intensities, but not the spectral resolution, of the resonance Raman spectrum. Thus, the resonance Raman intensities can reveal the vibrational mode-specific reorganization energies even in systems having completely diffuse absorption spectra.

Computational evaluation of eq 3 can be unreasonably time-consuming because of the number of levels $|v\rangle$ that must be considered for large molecules or those with dissociative excited states. This difficulty can be alleviated by applying a simple mathematical transformation to convert the resonance Raman amplitude to a fully equivalent time-dependent formulation:[12,26−28]

$$\sigma_{R,i\rightarrow f}(\omega_L) = \frac{8\pi(eM)^4\omega_L{\omega_S}^3}{9\hbar^2c^4} \times \sum_i P_i \left| \int_0^\infty dt\, \langle f|i(t)\rangle \exp[i(\omega_L + \omega_i - \omega_0)t - \gamma t/2] \right|^2 \quad (4)$$

where $|i(t)\rangle = \exp[-iH_{ex}t/\hbar]|i\rangle$, with H_{ex} being the Hamiltonian governing vibrational motion on the excited-state potential energy surface. The corresponding time domain expression for the one-photon optical absorption cross section at the same level of approximation is

$$\sigma_A(\omega) = \frac{4\pi(eM)^2\omega}{3\hbar c} \times \sum_i P_i \,\mathrm{Re} \int_0^\infty dt \langle i|i(t)\rangle \exp[i(\omega + \omega_i - \omega_0)t - \gamma t/2] \quad (5)$$

Figure 2 gives a pictorial representation of eqs 4 and 5. The electronic absorption band shape and the resonance Raman intensity depend on the time-varying overlaps $\langle i|i(t)\rangle$ and $\langle f|i(t)\rangle$, respectively. The time dependence of $|i(t)\rangle$ represents the motion of the nuclei after the potential energy function is instantaneously (on the time scale of vibrational motion) switched from that of the ground electronic state to that of the excited state. Thus, the initial, subvibrational period time dependence of $|i(t)\rangle$ reflects the motions of the atoms from their ground state equilibrium positions toward excited state equilibrium. If the excited state is bound, the atomic positions will undergo periodic but generally multidimensional motion on that surface, resulting in a complicated time dependence of the moving wave packet's overlap with itself at time zero, $\langle i|i(t)\rangle$. The Fourier transform of this overlap, which gives the absorption spectrum, should in principle contain peaks at frequencies corresponding to all the bound excited-state vibrations along which geometry changes occur, but these are often not resolvable due to many-mode and/or solvent dynamics or inhomogeneous broadening (see below). This is where the resonance Raman experiment becomes so useful. The intensity of each Raman transition depends on the overlap of $|i(t)\rangle$ with a different, identifiable final state, a projection of the complex motion of $|i(t)\rangle$ onto specific ground-state vibrational coordinates (for fundamentals and overtones) or pairs of coordinates (for combination band intensities). In general, those modes that undergo the largest excited-state geometry changes will exhibit the highest intensities.

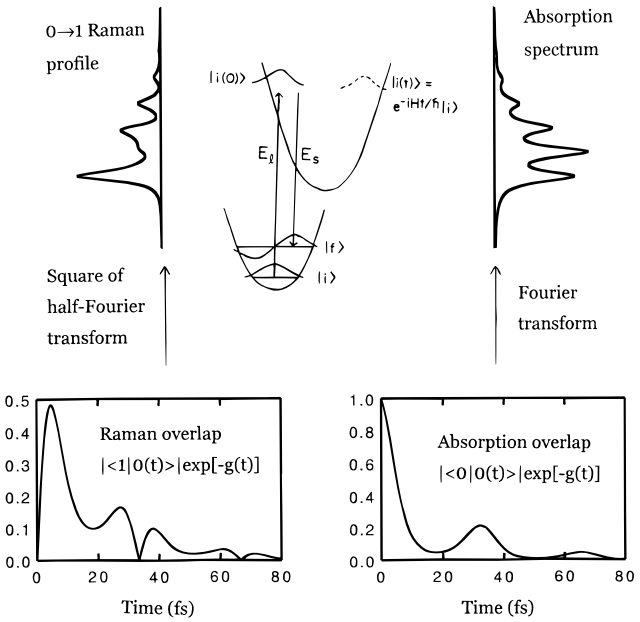

Figure 2. Formally time-dependent picture of steady-state resonance Raman and optical absorption spectroscopy for a one-mode system.

In polyatomic molecules, each overlap $\langle f|i(t)\rangle$ involves *all* vibrational coordinates. The overlap for a particular fundamental, for example, will be large only at those times when $|i(t)\rangle$ has evolved enough from $|i(0)\rangle$ to gain a good overlap with the ground-state wave function excited by one quantum in the mode of interest, yet still has good overlaps with the initial state in all of the other modes. The overall effect of motion along many vibrational modes is that the wave packet, once it leaves the neighborhood of the ground-state geometry, essentially never returns (*strictly* never returns for directly dissociative potentials), and both the absorption spectrum and the resonance Raman intensities become determined almost entirely by the dynamics occurring in the first tens of femtoseconds[15,27] (see Figure 3). Thus, the spectra of dissociative molecules, or those with many Franck−Condon active modes, depend mainly on just the first and/or second derivatives of the excited-state potential along the ground-state normal coordinates; anharmonicities do not influence the intensities strongly.

The demonstration that the Raman amplitude could be expressed as the half-Fourier transform of a time-dependent overlap, requiring no explicit summation over vibronic eigenstates, was a tremendous advance.[26,28,29] It made calculations on large molecules routinely feasible for the first time, as the computational effort in calculating and Fourier transforming the multidimensional overlaps in eq 4, particularly when the dynamics are assumed separable into products of each individual normal mode, is far less than that required to sum over all possible intermediate states in eq 3. It also facilitated calculations on large or dissociative molecules by emphasizing that such spectra are determined by only the *initial* motion of $|i(t)\rangle$ and thus require the excited-state surface only in the region near the ground-state geometry.

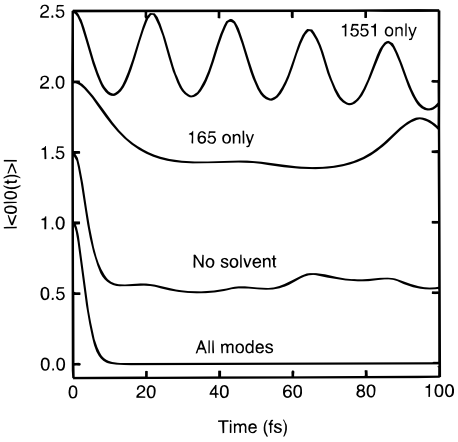

Figure 3. Overlap whose Fourier transform determines the zero-temperature optical absorption spectrum, $|\langle 0|0(t)\rangle|\exp[-g(t)]$, for the HMB/TCNE charge-transfer complex.[45] From top to bottom: overlap for the 1551 cm^{-1} mode only, with lifetime broadening alone; overlap for 165 cm^{-1} mode only, with lifetime broadening alone; overlap for all 11 Franck−Condon active vibrational modes, with lifetime broadening alone; overlap for all 11 vibrational modes with solvent reorganization and lifetime broadening. Each curve is successively displaced vertically by 0.5 units. As more degrees of freedom are included, the time during which the overlap differs significantly from zero becomes shorter.

The expressions given above assume isolated molecules. More precisely, they assume that the material system interacting with the light can be described fully by a state vector or wave function that spans all of the material degrees of freedom. In the solution phase, the electronically resonant molecules are surrounded by neighbors that have no resonant interaction with the radiation but perturb the chromophores that do. In this situation it is still most natural and practical to work in a basis of the eigenstates of the resonant chromophore, but due to the chromophores' interactions with the environment, the physics cannot be described by state vectors; a density matrix formulation is required. The description of any higher-order radiation−matter interaction then becomes considerably more involved because the time evolution of the bra- and the ket-sides of the density operator must be considered separately. Density matrix approaches to the calculation of monochromatically excited spontaneous emission (resonance Raman and fluorescence) have been given by a number of authors.[30−36] We have adopted the formalism of Mukamel and co-workers, who have developed a unified description of a wide variety of linear and nonlinear, frequency-domain and time-resolved spectroscopies.[34] For excitation on resonance with a single electronic state in the Condon approximation, the rate of detecting emitted photons at frequency ω_S, assuming monochromatic incident radiation of frequency ω_L, is

$$\sigma_{SLE}(\omega_L,\omega_S) = \frac{4\omega_L\omega_S{}^3M^4e^4}{9\hbar^2c^4}S_{SLE}(\omega_L,\omega_S) \qquad (6)$$

where

$$S_{SLE}(\omega_L,\omega_S) = 2\,\mathrm{Re}\int_0^\infty dt_3\int_0^\infty dt_2\int_0^\infty dt_1\{\exp(i\omega_L t_1 + i\omega_S t_3)R_1(t_3,t_2,t_1) + \exp(-i\omega_L t_1 + i\omega_S t_3)R_2(t_3,t_2,t_1) + \exp[-i\omega_L t_1 - i(\omega_L-\omega_S)t_2 + i\omega_S t_3]R_3(t_3,t_2,t_1)\} \qquad (7)$$

and

$$R_1(t_3,t_2,t_1) = \exp[-i\omega_0(t_3+t_1) - (\gamma/2)(t_3+t_1) - \gamma t_2]\times \exp[-g^*(t_3) - g(t_1) - f_+(t_3,t_2,t_1)] \qquad (8a)$$

$$R_2(t_3,t_2,t_1) = \exp[-i\omega_0(t_3-t_1) - (\gamma/2)(t_3+t_1) - \gamma t_2]\times \exp[-g^*(t_3) - g^*(t_1) + f_+{}^*(t_3,t_2,t_1)] \qquad (8b)$$

$$R_3(t_3,t_2,t_1) = \exp[-i\omega_0(t_3-t_1) - (\gamma/2)(t_3+t_1)]\times \exp[-g(t_3) - g^*(t_1) + f_-{}^*(t_3,t_2,t_1)] \qquad (8c)$$

$$f_-(t_3,t_2,t_1) = g(t_2) - g(t_2+t_3) - g(t_1+t_2) + g(t_1+t_2+t_3) \qquad (8d)$$

$$f_+(t_3,t_2,t_1) = g^*(t_2) - g^*(t_2+t_3) - g(t_1+t_2) + g(t_1+t_2+t_3) \qquad (8e)$$

The quantity $g(t)$ contains all information about the nuclear dynamics:

$$g(t) = g_{vib}(t) + g_{solv}(t) \qquad (9)$$

where $g_{vib}(t)$ is the contribution from the relatively high-frequency intramolecular vibrations of the chromophore and $g_{solv}(t)$ accounts for all low-frequency (or static) solvent or intermolecular modes that contribute to "pure dephasing" and/or "inhomogeneous broadening", depending on time scale.

Equation 7 imposes no artificial distinction between Raman and fluorescence and assumes no separation of time scales among the various processes that contribute to $g(t)$. It is, however, not very transparent, and its implementation is difficult for realistic models due to the computational effort required to evaluate the three nested time integrals. Fortunately, under many circumstances it can be simplified considerably. In near-room-temperature liquids and solids, where the environmental broadening of the electronic transitions is severe, the experimental emission spectrum usually appears to consist of readily distinguishable sharp "Raman" and broad "fluorescence" components. This implies that the two components ought to be separately calculable, and indeed this turns out to be approximately the case. As long as the system is in the rapid fluctuation limit, which means that the time scale for the solvent motions that broaden the electronic spectrum is much shorter than the ground-state vibrational dephasing time, one can approximately write the Raman-only part of the total emission in a form very similar to eq 4 apart from a change in the form of the electronic broadening function:[32]

$$S_{SLE}(\omega_L,\omega_S) = S_{Raman}(\omega_L,\omega_S) + S_{Fluor}(\omega_L,\omega_S) \qquad (10)$$

where

$$S_{Raman}(\omega_L,\omega_S) \propto M^4\omega_L\omega_S{}^3\times \sum_f\left|\int_0^\infty dt\langle f|i(t)\rangle\exp[i(\omega_L+\omega_i-\omega_0)t - g_{solv}(t) - \gamma t/2]\right|^2\times \delta(\omega_L-\omega_S-\omega_{fi}) \qquad (11)$$

and $S_{Fluor}(\omega_L,\omega_S)$ describes a usually much broader emission that underlies the sharp Raman spectrum. While the δ function is often replaced by some other function representing a realistic ground-state vibrational line shape, the separation that leads to eq 11 is rigorously correct only in the limit of vanishing vibrational line widths.[31] The result of eq 11 is essentially Heller's time-domain expression of eq 4, with an additional factor of $\exp[-g_{solv}(t)]$ which accounts for the role of solvent dynamics in damping the time-dependent wave packet overlaps.

Static (inhomogeneous) contributions to $g_{solv}(t)$ may also be incorporated by averaging the entire cross section over a distribution of electronic transition energies and/or other parameters. A Boltzmann distribution of initial vibrational states is handled similarly. The final results for the resonance Raman cross section and the absorption spectrum become

$$\sigma_{R,i\rightarrow f}(\omega_L) = \frac{8\pi(eM)^4\omega_L\omega_S^3}{9\hbar^2c^4}\sum_i P_i \int d\delta\, G(\delta) \times \left|\int_0^\infty dt\langle f|i(t)\rangle \exp[i(\omega_L + \omega_i - \omega_0 - \delta)t - g_{solv}(t)]\right|^2 \quad (12)$$

and

$$\sigma_A(\omega) = \frac{4\pi(eM)^2\omega}{3\hbar cn}\sum_i P_i \int d\delta\, G(\delta) \times \mathrm{Re}\int_0^\infty dt\langle i|i(t)\rangle \exp[i(\omega + \omega_i - \omega_0 - \delta)t - g_{solv}(t)] \quad (13)$$

where δ is the shift from the central zero−zero frequency and $G(\delta)$ describes the inhomogeneous distribution of these shifts. In eq 13, n is the solvent refractive index.[15] The requirement for this separation of the total emission into Raman and fluorescence components is that the "homogeneous" solvent dynamics described by $g_{solv}(t)$ are fast compared with the inverse ground-state vibrational line width, which determines the time scale for the entire Raman scattering process, while the "inhomogeneous" broadening is essentially static on this time scale. This is a useful separation, although necessarily an approximate one. The distinction is that homogeneous broadening *on the Raman time scale* affects the resonance Raman *amplitude*, while inhomogeneous broadening contributes to a distribution of *cross sections*.[15]

Finally, the band shape of the ordinary fluorescence spectrum, assuming complete solvent and vibrational relaxation to thermal equilibrium prior to emission, is given by the same expression as for the absorption band shape with the roles of upper and lower states reversed:[9]

$$I_F(\omega) \propto \omega^3 \sum_v P_v \int d\delta\, G(\delta) \times \mathrm{Re}\int_0^\infty dt\langle v|v(t)\rangle \exp[i(-\omega + \omega_v + \omega_0 + \delta)t - g_{solv}(t)] \quad (14)$$

Here, $|v\rangle$ is a vibrational level of the upper electronic state, and $|v(t)\rangle$ is that state propagated for time t by the ground-state vibrational Hamiltonian.

A variety of forms have been used in the literature for the solvent-induced homogeneous broadening. Probably the most useful simple model for application to charge-transfer transitions is the Brownian oscillator, which treats the solvent as one or more coupled vibrational modes each characterized by a frequency, a ground to excited-state displacement, and a frictional damping.[34,37−40] The friction can be varied continuously from the completely undamped harmonic oscillator typically used to describe high-frequency intramolecular vibrations to the overdamped relaxational degree of freedom generally used to describe collective solvation modes. For strongly overdamped modes, the dephasing function $g_{solv}(t)$ becomes

$$g_{solv}(t) = g'(t) + ig''(t) \quad (15)$$

where the real and imaginary parts are given by

$$g''(t) = -(\lambda/\Lambda)[\exp(-\Lambda t) + \Lambda t - 1] \quad (16a)$$

$$g'(t) = (\lambda/\Lambda)\cot(\hbar\beta\Lambda/2)[\exp(-\Lambda t) + \Lambda t - 1] + \frac{4\lambda\Lambda}{\hbar\beta}\sum_{n=1}^{\infty}\frac{\exp(-\nu_n t) + \nu_n t - 1}{\nu_n(\nu_n^2 - \Lambda^2)} \quad (16b)$$

Here λ and Λ are the Stokes shift and the inverse time scale, respectively; the time scale for a given Brownian oscillator mode is related to the frequency of the oscillator, ω_{BO}, and its friction, γ, by $\Lambda = \omega_{BO}^2/\gamma$. β is $1/k_BT$ and the parameter ν_n in eq 16b is equal to $2\pi n/\hbar\beta$. In the high-temperature limit ($k_BT \gg \hbar\Lambda$), eq 15 simplifies to

$$g_{solv}(t) = (2\lambda k_BT/\hbar\Lambda^2)[\exp(-\Lambda t) + \Lambda t - 1] - i(\lambda/\Lambda)[\exp(-\Lambda t) + \Lambda t - 1] \quad (17)$$

In this high-temperature, strongly overdamped limit, the solvent-induced line shape becomes Gaussian with a standard deviation given by $(2\lambda k_BT/\hbar)^{1/2}$ in agreement with classical Marcus theory.

Applications

Noncovalent Charge-Transfer Molecules. *Hexamethylbenzene/Tetracyanoethylene.* The charge-transfer complex most widely studied by resonance Raman techniques is that between hexamethylbenzene (HMB) as the electron donor and tetracyanoethylene (TCNE) as the acceptor. This system forms a ground-state complex with a large equilibrium constant that absorbs fairly strongly in the middle of the visible spectrum ($\lambda_{max} \approx$ 540 nm and $\epsilon_{max} \approx 4200$ M^{-1} cm^{-1} in CCl_4), far from any locally excited transitions of donor or acceptor. The equilibrium constants and dipole moments of both the 1:1 and the 2:1 (DAD) complexes and the electronic and vibrational spectroscopy of this complex have been studied extensively in a variety of solvents. Several vibrations of this complex were also the subject of a very early resonance Raman excitation profile study.[41] Other resonance Raman studies have focused on the low-frequency, presumed intermolecular stretching mode of this complex[42] and related complexes of TCNE with other donors.[43]

Our group's initial study obtained absolute excitation profiles for 11 fundamentals, which included modes localized on both the donor and the acceptor as well as the low-frequency presumed intermolecular stretch mode.[44] A number of overtones and combination bands were also observed (Figure 4). We then simulated the absorption spectrum and excitation profiles in CCl_4 with a model that explicitly included all 11 fundamentals plus an overdamped Brownian oscillator to represent the solvent. The original analysis did not make use of the information present in the fluorescence spectrum; its maximum is near 890 nm and the quantum yield is only about 5×10^{-5}, making this a nontrivial measurement. The best fit yielded reasonable values for the internal reorganization energies, but the electronic zero−zero energy of 11 600 cm^{-1} appeared too low to be consistent with known oxidation and reduction potentials, and the "solvent" reorganization energy of 3930 cm^{-1} seemed far too large for a nonpolar solvent.

Subsequent incorporation of the weak, far-red fluorescence spectrum to constrain the model (Figures 5 and 6) resulted in a considerably higher zero−zero energy (13900 cm^{-1}) and lower total reorganization energy, but the relative weakness of the observable resonance Raman lines above 100 cm^{-1} still required a large amount of electronic spectral broadening, presumably due to reorganization along unobserved, low-frequency motions.[45] This apparent solvent reorganization energy of 2450

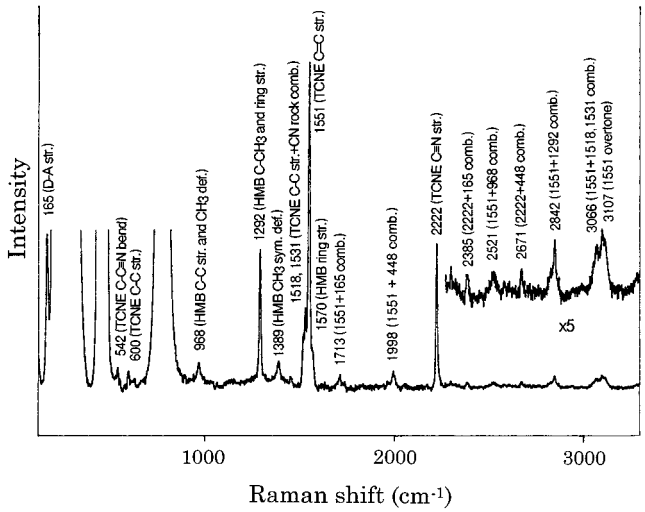

Figure 4. Resonance Raman spectrum of the HMB/TCNE charge-transfer complex in CCl_4 solvent at 514 nm excitation. Resonance-enhanced vibrations of the complex are labeled with their approximate mode descriptions. Experimental conditions are described in ref 44.

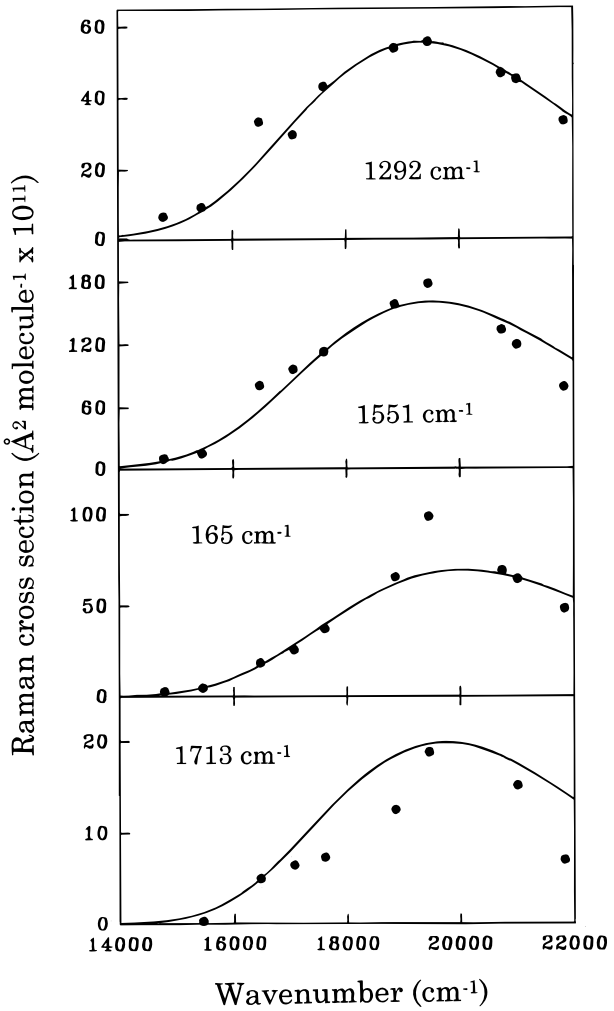

Figure 5. Experimental (points) and calculated (curves) resonance Raman excitation profiles for four vibrations of the HMB/TCNE charge-transfer complex in CCl_4: a donor-localized fundamental (1292 cm^{-1}), an acceptor-localized fundamental (1551 cm^{-1}), the presumed intermolecular stretching fundamental (165 cm^{-1}), and a combination band (1713 cm^{-1}). Parameters of the simulations are given in ref 45.

cm^{-1}, far greater than that predicted by simple dielectric continuum theories (approximately zero), has been the subject

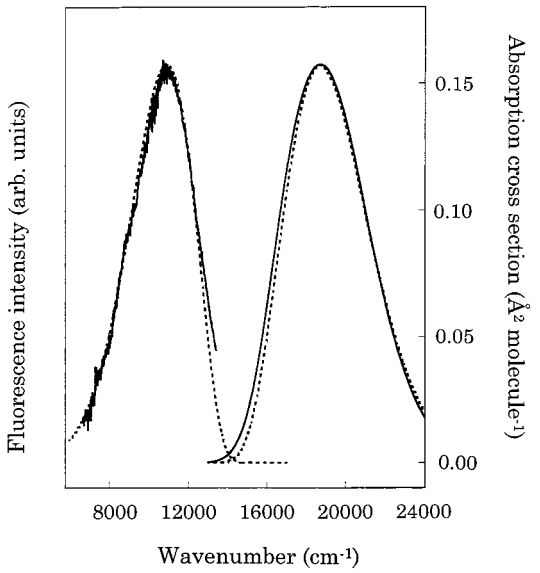

Figure 6. Experimental (solid) and calculated (dashed) absorption spectra and fluorescence band shapes for the HMB/TCNE charge-transfer complex in CCl_4. Parameters of the simulations are given in ref 45.

of some controversy. Some of it may be attributable to the other five low-frequency intermolecular modes that are not observed in the Raman spectrum. However, there is increasing evidence that the true solvent contribution to reorganization energies is significant even for completely non(di-)polar solvents.[46,47] Even rigid aromatic molecules known to have no low-frequency Franck−Condon active vibrations typically exhibit Stokes shifts between absorption and fluorescence apparent origin band maxima of at least a few hundred wavenumbers in room-temperature liquid solvents. The "viscoelastic" contribution to solvent reorganization which arises purely from the change in effective size of the solute upon electronic excitation has been addressed in detail by Berg both experimentally and theoretically[48−50] and in recent simulations by Schwartz and coworkers.[51] This mechanism could be particularly important in noncovalent CT complexes where the intermolecular separation might be expected to change significantly upon excitation from the neutral to the ion pair state. Finally, recent photoacoustic calorimetric studies by the Braslavsky group indicate a very large contribution from electrostriction to the energetics of CT transitions even in nonpolar (alkane) solvents.[52] In HMB/TCNE, the Stokes shift between absorption and fluorescence maxima is nearly 800 cm^{-1} larger in CCl_4 than in cyclohexane, suggesting a significant contribution from the solvent itself to the total low-frequency reorganization energy.[45] Resonance Raman studies of molecular ions in polar solvents[53,54] and intramolecular charge-transfer molecules[55−57] also provide a variety of evidence for coupling of nominally chromophore-localized electronic transitions to specific internal vibrations of the solvent. The magnitude and origin of solvent contributions to the reorganization energy (or, equivalently, the electronic spectral breadth) remains a topic of active study in regard to molecular electronic transitions in general, not only charge-transfer phenomena.

The same model for the vibrational dynamics was used to calculate the nonphotochemical return electron-transfer rate[58] for comparison with previous direct and indirect measurements of the ion pair lifetime carried out both by our group and by others.[59−61] This requires a value for the electronic coupling matrix element, which can in principle be obtained from the spectroscopic transition moment following the Mulliken−Hush prescription or one of its variations.[1,4,5,62,63] In this system, there

is a complication in that the radiative rate calculated from the experimental ion pair lifetime and fluorescence yield is about a factor of 4 smaller than that estimated from the integrated absorption strength. This breakdown of the Strickler−Berg relations that connect absorption strength with emission lifetime and quantum yield[64] suggests that the relaxed ion pair state may be very different from the vertically excited charge-transfer state in these conformationally labile noncovalent complexes. That is, there is a significant change in the electronic coupling between the absorbing and emitting states presumably due to the large geometry change (a non-Condon effect), which may be a rather general feature of charge-transfer transitions. In any case, regardless of whether the absorption or the fluorescence transition moment is used to estimate the electronic coupling, the calculated return electron transfer process is significantly faster than observed. This nevertheless represents the first time, to our knowledge, that a serious attempt has been made to simulate all four pieces of data (absorption, fluorescence, Raman, and return electron-transfer rate) with a common model for comparison with experimental results.

We also examined the spectroscopy of the complex with perdeuterated hexamethylbenzene (HMB-d_{18})[58] in the hope of shedding some light on the unexpectedly large isotope effect on the return electron-transfer rates of this and many related systems.[60,65−68] The vibrations that carry significant intensity in the resonance Raman spectra are only slightly shifted by perdeuteriation of the HMB, suggesting that hydrogen motions are only weakly coupled to the charge-transfer transition. However, both fluorescence quantum yields and direct time-resolved pump−probe measurements of ground-state recovery times indicate that perdeuteriation decreases the rate of non-photochemical return electron transfer by a factor of about 1.6, implying more significant participation of modes involving hydrogen motion. Calculations within the harmonic approximation were unable to reproduce the isotope effects on both the spectra and the kinetics with a common set of parameters. Large deuterium isotope effects (often much larger than those observed here) are seen in the rates of many other organic radiationless transitions and have been attributed to anharmonicities of the CH (CD) stretches, which render these important accepting modes even though they do not appear to carry Franck−Condon activity in the absorption or emission spectra.[69,70] We are, however, dubious about this explanation in light of the comparatively small electronic energy gap (as radiationless transitions go) and the extensive Franck−Condon activity in many of the non-CH stretching modes. This issue clearly has yet to be resolved.

McHale and co-workers also examined the HMB/TCNE complex using CH_2Cl_2 as the solvent.[71] They measured more detailed excitation profiles, but for only the four strongest resonance Raman lines. These four modes of the complex and a stochastic line broadening function for the solvent were employed to explicitly model the absorption spectrum and excitation profiles. Their experimental excitation profiles all peaked above 20 000 cm^{-1}, considerably blue-shifted relative to the profiles measured by our group in CCl_4 and the absorption spectra in both solvents, and large non-Condon couplings had to be included in the model in order to fit these profiles. They also obtained a large low-frequency reorganization energy of about 6200 cm^{-1}, which is probably best considered as representing some combination of true solvent contributions, reorganization of the high-frequency molecular modes not included in the simulations, and reorganization of unseen low-frequency intermolecular modes. These authors concluded, from the solvent dependence of the excitation profiles together with a variety of other observations, that the ground-state structure of the complex in CH_2Cl_2 is less symmetric than that in CCl_4, allowing mixing with and intensity borrowing from locally excited states of TCNE in the latter solvent. Indeed, much current thinking in the charge-transfer field calls into question the simple Mulliken picture which considers only two electronic states, the neutral ground state and the ion pair.

A lingering question regarding this system is the possible contribution of multiple charge-transfer transitions to the spectroscopy and dynamics. The HOMO of HMB, from which the optically promoted electron nominally comes, is degenerate in free HMB, but that degeneracy should be broken by complexation with an acceptor. Many substituted benzene/TCNE complexes do clearly exhibit two CT bands in the visible region of the spectrum.[72−74] Therefore, one might expect the HMB/TCNE charge-transfer electronic spectrum to consist of two transitions, both polarized roughly along the internuclear axis and of similar character, but split by some amount too small to be evident in the solvent-broadened absorption spectrum. The presence of two transitions, assuming both states absorb while only the lower one emits, could contribute to the apparent Stokes shift and cause the solvent reorganization energy to be overestimated. The resonance Raman excitation profiles exhibit none of the interference features often generated by two overlapping electronic states,[75,76] but again the spectral simulations suggest that this is not inconsistent with the two transitions of similar electronic character. McHale and co-workers did observe such interferences in the 2:1 DAD complex of HMB with TCNE in cyclohexane, and attributed them to the two different charge-transfer states originating from the two different localized D−A transitions in the complex.[77] Hayashi et al. used the INDO/S semiempirical method to calculate a splitting of 400 cm^{-1} between the two CT states, and after making assumptions about the relative reorganization energies and transition moments in the two states, were able to reproduce the experimental absorption and fluorescence spectra as well as various ultrafast time-resolved data.[78,79] McHale and co-workers carried out INDO calculations of the spectra and potential energy surfaces of HMB/TCNE and found that both the splitting between the two CT states and their relative oscillator strengths are strong functions of the complex geometry, which is expected to be quite floppy in the solution phase and may vary from one solvent to the next.[71]

While charge transfer in complexes involving TCNE has been studied widely by both resonance Raman and other techniques, to our knowledge no one has yet carried out the detailed normal-mode analysis needed to convert the dimensionless normal mode reorganization energies into actual bond length and bond angle changes as described below for 1-aza-adamantane-4-yliden-emalononitrile, even though the required normal-mode analysis for a molecule as simple as TCNE is fairly straightforward. For a pure quasidiatomic stretch, the relationship between dimensionless normal mode displacement Δ and bond length change δr is $\delta r = (\hbar/\mu\omega)^{1/2}\Delta$, where μ is the reduced mass for the vibration and ω is its frequency in s^{-1}. Using $\lambda = \varpi\Delta^2/2$ (valid when the ground- and excited-state vibrational frequencies are assumed to be the same), where ϖ is the wavenumber of the normal mode and λ is that mode's reorganization energy in wavenumbers, we obtain the relationship $\delta r = (2\lambda\hbar/\mu\omega\varpi)^{1/2}$. If the ∼1550 cm^{-1} mode of TCNE is taken to be a pure CC stretch and this is assumed to be the only normal mode that has ethylenic C═C stretching character, then the bond length change in centimeters becomes $\delta r = (2.1 \times 10^{-11})\lambda^{1/2}$, which

TABLE 1: Summary of Vibrational and Solvent Contributions to Charge-Transfer Reorganization Energies

molecule	solvent	λ_V (cm^{-1})[a]	λ_S (cm^{-1})[b]	$\lambda_{C=C}$ (cm^{-1})[c]
hexamethylbenzene/tetracyanoethylene (ref 45)	CCl_4	2266	2450	685
hexamethylbenzene/tetracyanoethylene (ref 71)	CH_2Cl_2	1567	6200	338
p-methoxybenzyltrimethylsilane/tetracyanoethylene (ref 87)	CH_2Cl_2	2032	2820	860
1-aza-adamantane-4-ylidenemalononitrile (ref 106)	CH_3OH	3490	1032	821
1-aza-adamantane-4-ylidenemalononitrile (refs 82 and 83)	CH_3CN	2575	225	426

[a] Total reorganization energy in all resolved molecular vibrations. [b] "Fast" part of solvent reorganization energy (not including inhomogeneous broadening). [c] Reorganization energy in ~1550 cm^{-1} C=C stretch of TCNE or dicyanovinyl group.

ranges from 0.04 to 0.06 Å for the reorganization energies given in Table 1. These bond length changes are in reasonable agreement with the values of 0.08 Å calculated ab initio[80] and 0.04 Å found from the crystal structure of the salt of $TCNE^{\bullet-}$ with $[Fe(C_5Me_5)_2]^{\bullet+}$.[81] For the closely related dicyanovinyl-substituted aza-adamantane intramolecular charge-transfer molecule discussed below, we did calculate the geometry changes upon charge-transfer excitation in the correct way using the normal mode coefficients of all the reorganized modes and obtained a C=C bond length increase of 0.04 Å,[82,83] in good agreement with the simple quasidiatomic estimates for TCNE.

Methoxybenzyltrimethylsilane/TCNE and Phenylcyclopropane/TCNE. HMB/TCNE was selected for our initial studies because of its favorable thermodynamic and spectroscopic properties, not because this complex itself is of intrinsic interest. The experiments on HMB/TCNE were intended to test fundamental relationships between spectroscopic observables and electron transfer rates, and the most experimentally tractable systems for studies of this type are those in which the energy of the absorbed photon is ultimately dissipated as heat or returned as fluorescence without initiating any chemistry. However, useful applications of photoinduced electron transfer often involve harnessing the energy of the ion pair state to initiate a chemical reaction. We therefore looked to adapt the methodologies developed and refined on HMB/TCNE to systems in which one member of the ion pair formed by photoinduced charge transfer (the cation in this case) is chemically reactive.

The systems chosen for initial study were the CT complexes formed between TCNE as an acceptor and benzyltrialkylsilanes or phenylcyclopropanes as donors. The radical cations of both electron donors exhibit high chemical reactivity compared with the corresponding neutrals; the benzyltrialkylsilanes undergo facile cleavage of the C−Si bond via a nucleophilic S_N2 mechanism,[84] while the phenylcyclopropanes undergo rapid ring opening.[85,86] One important goal of this study was to explore the extent to which the radical cation initially formed by CT excitation is the same species that undergoes subsequent chemical reaction. Direct CT excitation is expected to involve primarily the molecular orbitals on the aromatic ring; does this phenyl-centered ion radical later evolve to a species having more positive charge on the reactive silyl or cyclopropyl group, and if so, through what mechanism?

This question was addressed by combining absorption and resonance Raman spectral modeling of the donor/TCNE CT complex, which provides information about the vertically excited CT state, with pump−probe measurements in which the donor radical cation was prepared by electron transfer from a photoexcited sensitizer and the resonance Raman spectrum of the relaxed radical cation was subsequently measured. The pump−probe resonance Raman spectra of the *p*-methoxybenzyltrimethylsilane radical cation exhibit more than 20 frequencies which, assigned through a combination of density functional theory calculations and isotopic substitution, indicate significant weakening of the benzyl C−Si bond that becomes reactive in the radical cation.[87] The pump−probe resonance Raman spectra of phenylcyclopropane also revealed a number of vibrational frequencies of the radical cation, but they were considerably more difficult to assign in the absence of data on isotopically substituted molecules.[88] The resonance Raman experiments on the ground-state donor/TCNE CT complexes were, unfortunately, not definitive in either system due to the less-than-ideal thermodynamic and spectroscopic properties of these complexes. The combination of small equilibrium constants for complex formation and low molar absorptivities for the complex results in the CT-resonant Raman spectra being dominated by solvent lines and nonresonant scattering from uncomplexed donor and acceptor, obscuring a number of potentially interesting Raman lines and making quantitative analysis of the spectra uncertain. Our best efforts to model the spectra of *p*-methyoxybenzyltrimethylsilane/ TCNE resulted in reorganization energies of the TCNE acceptor modes that are similar to those obtained in HMB/TCNE (860 cm^{-1} in the C=C stretch and 300 cm^{-1} in C≡N stretching) and a reasonable solvent reorganization energy of 2820 cm^{-1} in CH_2Cl_2, providing some confidence in the modeling results.[87] Of the five observed resonance-enhanced silane vibrations, four are largely localized on the aromatic ring. This strongly suggests that the reorganization parameters obtained from analysis of the CT-resonant Raman spectra do not properly describe the structure of the relaxed, solvent-separated radical cation, but we are unable to determine whether the mechanism enabling this structural evolution involves an electronic nonadiabatic transition, strongly anharmonic vibrations of the silane itself such as internal rotations, or coupling of the silane geometry to ion pair separation or solvent reorganization. In phenylcyclopropane/TCNE, we clearly observed, in addition to the TCNE C=C and C≡N stretches, only three resonance-enhanced vibrations of the donor, all phenyl-localized (Figure 7). No effort was made to quantitatively model the very weak and sparse spectra, but qualitatively they are again consistent with vertical CT excitation being largely localized on the aromatic ring rather than on the eventually reactive substituent.

Carbazole/Tetracyanoethylene. While some of the useful applications of photoinduced charge transfer result in chemical reactions of the primary electron donor and/or acceptor, many others involve only charge transport without any net chemistry. In photosynthesis, for example, the initial light-driven charge separation is followed by a cascade of electron transfer steps that separate the electron from the hole, preventing energy-wasting charge recombination and allowing time for the slower chemical steps to proceed. In electrophotography (xerography), electrons and holes produced by light absorption are separated by charge hopping in an external electric field, with the separated charges eventually being used to charge a platen that attracts the toner electrostatically and produces the image on paper. In organic light-emitting diodes, electrons and holes injected at opposite sides of the device must migrate toward the center where they recombine to form excitons which emit light. In all

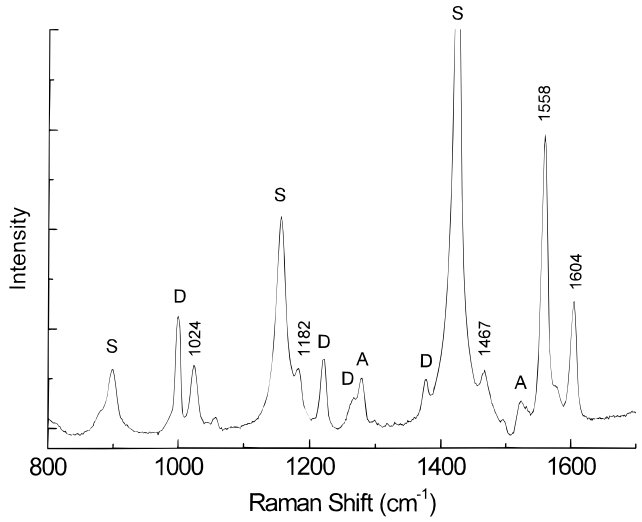

Figure 7. Resonance Raman spectrum of the phenylcyclopropane/TCNE charge-transfer complex in CH_2Cl_2 at 488 nm. The five frequencies labeled are those that appear to exhibit some degree of resonance enhancement. The 1558 cm^{-1} line is the C═C stretch of TCNE, while the lines at 1024, 1182, and 1604 cm^{-1} are assigned to phenyl-based donor modes. The 1467 cm^{-1} line is assigned as a donor mode having some contribution from cyclopropyl ring breathing, which is only weakly if at all resonance enhanced. S labels solvent lines and D and A mark vibrations of uncomplexed donor and acceptor, respectively, that do not exhibit resonance enhancement in the complex. More detailed assignments of the phenylcyclopropane modes are given in ref 88.

of these systems the important steps involve hopping of electrons or holes between nearby molecules in the dark.

Although the processes of greatest interest in these systems are not the directly light-driven ones, resonance Raman intensity analysis of photoinduced charge-transfer transitions can still provide useful information about the material parameters that determine these rates. Charge separation in electrophotography, for example, involves hole hopping between donor molecules D embedded in an amorphous solid matrix,[89] $D^{\bullet+} + D \rightarrow D + D^{\bullet+}$. The rate of this process depends on the applied electric field, the electronic coupling (orbital overlap) between the active molecular orbitals on neighboring molecules, the degree of energetic disorder among donor molecules sitting in different sites in the matrix, and the reorganization energy accompanying the hole transfer.[90−94] The internal reorganization energy for the donor molecules can be obtained to a good approximation from resonance Raman intensity analysis of a CT complex between D and a suitable acceptor, $D/A + h\nu \rightarrow D^{\bullet+}/A^{\bullet-}$. This analysis will also produce values for the reorganization energy of the surrounding matrix and for the degree of inhomogeneous broadening (i.e., energetic disorder). While these values pertain to charge separation in the D/A complex and not to charge transfer from one donor to another, they presumably provide at least some estimate of the matrix reorganization energy and energetic disorder parameter needed to calculate the actual rate of charge hopping.

With this application in mind, we initiated studies of the carbazole/TCNE charge-transfer complex (Figure 8). This system was selected because hole transport in isopropyl carbazole, as well as polymers containing carbazole side chains, has been studied in some detail;[95,96] we chose unsubstituted carbazole because the thermodynamic and spectroscopic properties of its complex with TCNE had already been reported[74] and because the vibrational assignments were expected to be much more straightforward for the unsubstituted molecule.[97] The

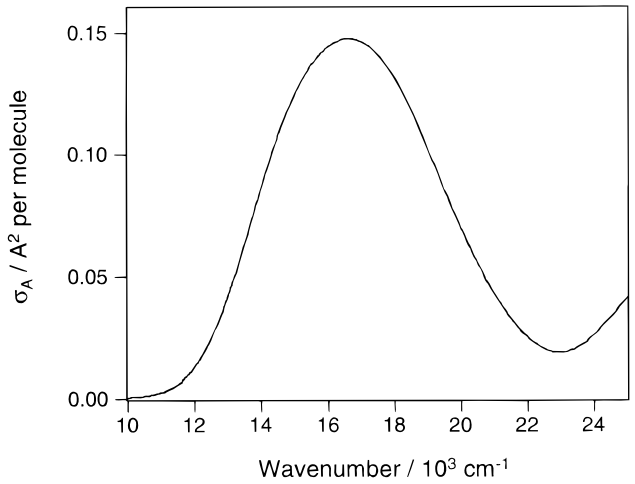

Figure 8. Absorption spectrum of the carbazole/TCNE charge-transfer complex in CH_2Cl_2.

equilibrium constant for carbazole/TCNE is considerably smaller than that of HMB/TCNE, but it is large enough, and the molar absorptivity of the complex high enough to produce a reasonably strong resonance Raman spectrum with only modest contamination from nonresonant Raman lines of uncomplexed donor and acceptor (Figure 9). One complication with carbazole is the clear existence of two overlapping charge-transfer electronic transitions, which are well characterized as resulting from promotion of an electron from the HOMO and the HOMO-1 of carbazole.[74] The absorption and resonance Raman spectroscopic analysis of this complex therefore required refining the methodologies for treating overlapping electronic transitions which we initially developed for and applied to the CT and LE transitions of 1-aza-adamantane-4-ylidenemalononitrile, discussed below. This analysis has recently been completed.[98]

Intramolecular Charge-Transfer Molecules. *1-Aza-Adamantane-4-Ylidenemalononitrile.* Noncovalent charge-transfer complexes have the advantage of allowing easy mixing and matching of donors and acceptors without synthetic effort. There are, however, a number of disadvantages to working with such complexes, including the possibility of multiple ground-state conformers and/or complex stoichiometries and of very large changes in intermolecular geometry between the neutral and ion-pair states. Also, it is difficult to obtain the highly accurate values for the equilibrium constants and molar absorptivities needed for quantitative analysis of the resonance Raman intensities. For these reasons, compounds bearing covalently attached electron donor and acceptor groups are quite attractive. A wide variety of such molecules have been synthesized, mostly for the purpose of studying the distance dependence of electron-transfer rates.[22,99] The goal of most such studies is to locally excite either the donor or the acceptor alone and measure the rate of decay of the initially excited state or the rate of formation of the ion(s), and it is desirable to have weak electronic coupling between donor and acceptor such that direct charge-transfer excitation does not complicate the picture and so that the electron-transfer rate is slow enough to measure accurately. It is, however, entirely possible to synthesize intramolecular donor−acceptor molecules with sufficiently large electronic coupling to provide a strong charge-transfer band.[100,101] Large electronic coupling is also desirable in the "push−pull" conjugated chromophores being developed for their nonlinear optical properties.[102−104] Our group has examined several such covalent donor−acceptor molecules. 1-Aza-adamantane-4-ylidenemalononitrile, synthesized by the Verhoeven group, shows a fairly strong charge-transfer band ($\lambda_{max} \approx 320$ nm and

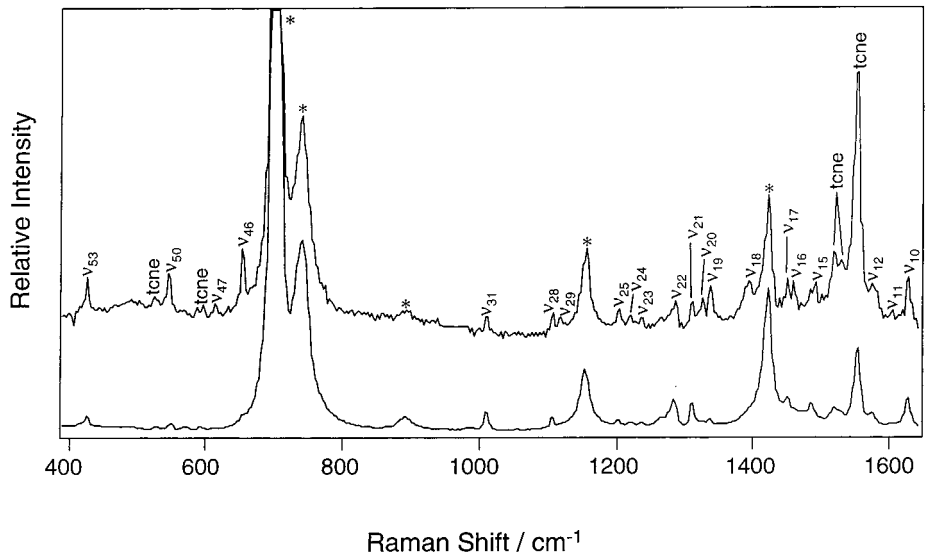

Figure 9. Resonance Raman spectra of the carbazole/TCNE charge-transfer complex in CH_2Cl_2 at excitation wavelengths near the red sides of the absorption band (687 nm, upper spectrum) and near the blue side (488 nm, lower spectrum). Asterisks mark solvent bands. The large excitation wavelength dependence of the intensities of some lines is consistent with the contribution of more than one electronic transition to the charge-transfer band of Figure 8.

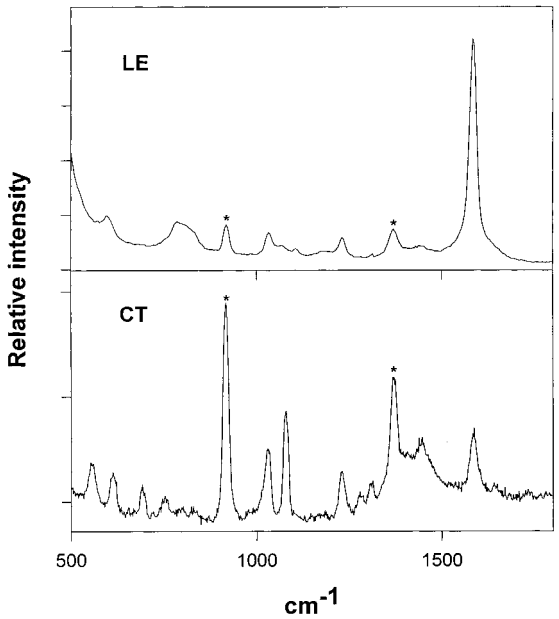

Figure 10. Resonance Raman spectra of 1-aza-adamantane-4-yliden-emalononitrile in acetonitrile solution excited on resonance with the locally (acceptor end) excited transition (239 nm) and with the charge-transfer transition (309 nm). Asterisks mark solvent bands.

$\epsilon_{max} \approx 4500\ M^{-1}\ cm^{-1}$) in a region of the spectrum where neither the donor-only nor the acceptor-only analogues absorb, and the fluorescence from this state exhibits the large solvatochromic shifts diagnostic of a charge-transfer transition.[105] At least 18 vibrational fundamentals exhibit Raman intensity on resonance with this charge-transfer band[82,106] (see Figure 10). These vibrations have been assigned through resonant and nonresonant Raman and infrared spectra, ab initio calculations, and comparison with model compounds.[107] The donor-only and acceptor-only analogues were also prepared and shown to exhibit negligible Raman intensity when excited at the same wavelengths used to obtain charge-transfer resonant spectra of the donor−acceptor compound.[106] The principal difficulty in working with this molecule was the rather strong relaxed fluorescence, which prevented us from performing Raman experiments in nonpolar or weakly polar solvents where the Stokes shift is small. Our initial resonance Raman experiments were carried out in methanol, a solvent in which the fluorescence is particularly weak (the fluorescence decay was too fast to resolve by time-correlated single-photon counting, indicating a lifetime shorter than about 20 ps), and were performed at a single excitation wavelength slightly to the red of the absorption maximum.[106] The resonance Raman intensities and absorption spectra were modeled as described for hexamethylbenzene/tetracyanoethylene to determine the intramolecular and solvent contributions to the reorganization energy accompanying electron transfer. The spectral fitting in methanol required a fairly large contribution from solvent-induced broadening that is inhomogeneous on the Raman time scale. Interestingly, calculation of the fluorescence spectrum under the assumption that this inhomogeneous component remains static on the longer fluorescence time scale results in severe underestimation of the Stokes shift. In the opposite limit, where the "inhomogeneous" broadening is attributed entirely to solvent oscillators that do relax completely prior to fluorescence as in the usual liquid-phase Marcus theory, the Stokes shift is overestimated (see Figure 11). This implies that the solvent-induced broadening in methanol has components that fluctuate on a wide range of time scales, perhaps related to the hydrogen-bonding dynamics in this solvent. The absorption spectrum in methanol also happens to be somewhat blue-shifted relative to other solvents of comparable polarity, suggesting the importance of more specific hydrogen-bonding interactions. A more detailed analysis was performed on this compound in acetonitrile solution.[82] Absolute scattering cross sections were measured at five excitation wavelengths spanning both the charge-transfer (CT) band at 324 nm and the lowest locally excited (LE) band at 231 nm. The spectra are qualitatively quite different; the LE-resonant spectra are dominated by the C═C and C≡N stretching modes of the acceptor group, while the CT-resonant spectra show intensity in a large number of vibrations localized on both the donor and acceptor groups as well as the adamantane bridge. The geometry changes accompanying both LE and CT excitation were quantitated by modeling the absorption spectra and resonance Raman intensities self-consistently to obtain the mode-specific reorganization energies accompanying electronic excitation to both states, using a modification of eq 12 that

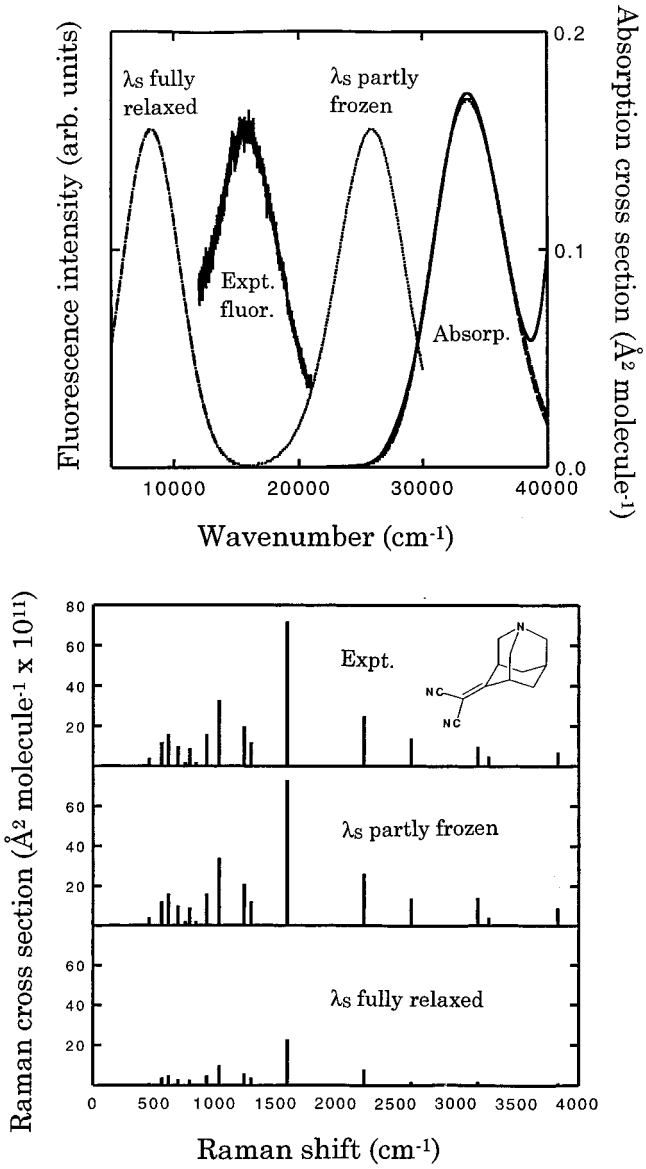

Figure 11. Absorption spectra, fluorescence band shapes, and resonance Raman intensities calculated for 1-aza-adamantane-4-ylidenemalononitrile in methanol employing different assumptions about time scales for solvent reorganization. The "λ_S partly frozen" curves partition the solvent-induced broadening into inhomogeneous (completely static distribution of zero−zero energies) and homogeneous (rapidly reorganizing) contributions to best reproduce the absolute resonance Raman cross sections (bottom panel). This underestimates the fluorescence Stokes shift (top panel). The "λ_S fully relaxed" curves assign all the solvent-induced broadening as rapidly reorganizing. This overestimates the fluorescence Stokes shift and produces too much damping of the resonance Raman cross sections. Both calculations accurately reproduce the experimental absorption spectrum (top panel). The conclusion is that the total solvent reorganization consists of one component that is fast on the Raman time scale, one that is slow on the Raman time scale but fast compared with fluorescence, and one that is static on the fluorescence time scale. Parameters of the simulations are given in ref 106.

includes interference effects between the two states. These were found to be of minimal importance for this particular charge-transfer molecule. We did, however, find that non-Condon effects (coordinate dependence of the electronic transition moment) had to be included in order to adequately simulate the data.

The reorganization parameters in terms of dimensionless normal coordinates, for both the LE and CT states, were then converted to actual bond length and bond angle changes by making use of a detailed ground-state normal-mode analysis[107] and by comparing with electronic structure calculations on models for the donor and acceptor ends to reduce the indeterminacy in the signs of the dimensionless displacements.[82,83,108] As expected from qualitative inspection of the resonance Raman spectra, the geometry changes upon excitation to the LE state were shown to be dominated by lengthening of the ethylenic C=C bond, while for CT excitation the distortions are distributed over the donor, acceptor, and adamantane bridge (Figure 12). The C=C bond length change is 0.04 Å for CT excitation and 0.07 Å for LE excitation. This is qualitatively consistent with a simple orbital picture in which LE excitation corresponds to moving an electron from the π orbital of the dicyanovinyl group into the π^* orbital of the same group, while CT excitation removes an electron from the aza-adamantane nitrogen lone pair and places it into the π^* orbital of the acceptor. We believe this represents the first time that resonance Raman intensity analysis has been used to quantitate the geometry changes in both LE and CT states of the same molecule.

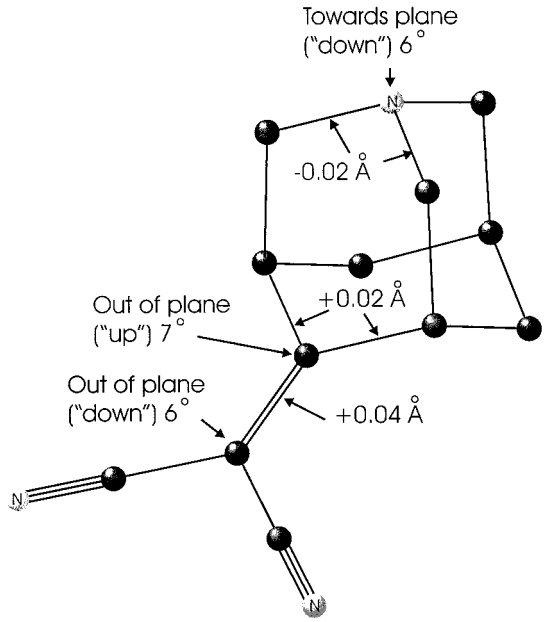

Figure 12. Geometry changes accompanying charge-transfer excitation of 1-aza-adamantane-4-ylidenemalononitrile in acetonitrile solution. All bond length changes exceeding 0.02 Å are shown, as are the three largest changes in dihedral angles expressed as the wagging angle about the indicated central atom. The structure shown is that calculated for the ground state, in which the wagging angles for the two ethylenic carbon atoms are approximately 0° while that for the aza-nitrogen is 53°. Details are given in refs 82 and 83.

Conclusions

In favorable cases, the self-consistent analysis of charge-transfer absorption band shapes and resonance Raman spectra can provide a wealth of detail about the internal vibrational contributions to the charge-transfer reorganization energy. When absolute resonance Raman intensities and/or the charge-transfer fluorescence band shape are also available, the analysis can also extract considerable information about the magnitudes and time scales of solvent reorganization processes. That being said, it should also be noted that the corresponding nonradiative return electron transfer rates are not very sensitive to the vibrational composition of the total reorganization energy, so this highly mode-specific information is not needed if one's only interest is in calculating the Franck−Condon contribution to the rate expression. One can reasonably argue that more detailed mode-

by-mode knowledge of the reorganization parameters should be helpful in the rational design of molecular or supramolecular structures with desirable electron-transfer properties, but this has yet to be demonstrated.

Resonance Raman intensity analysis is a finicky technique that places rather strict requirements on the photophysical properties of the molecular system. Features common to many interesting and/or important electron transfer systems such as weak or nonexistent charge-transfer absorption and/or emission bands, multiple overlapping electronic states, and vibrationally complex chromophores often make resonance Raman spectra difficult or impossible to obtain and/or analyze. Many time-domain pump−probe techniques performed with ultrashort (subvibrational period) laser pulses also contain information about the vibrational frequencies coupled to the electronic transition.[59,109−111] Some of these techniques appear to be more broadly applicable than spontaneous resonance Raman, although their analysis is often not as straightforward as might have originally been thought.[112] Clearly the maximum amount of information will be obtained by applying as many different spectroscopic, kinetic, and theoretical (e.g., electronic structure) methods as possible to each charge-transfer system of interest and then developing a model for the photophysics that is consistent with all of the available data. This is likely to require (and, one hopes, encourage) extensive collaboration among different research groups that are experts in different techniques.

Acknowledgment. This work was supported by grants from the NSF to A.M.K. (CHE-9708382) and to the Science and Technology Center for Photoinduced Charge Transfer at the University of Rochester (CHE-9120001). It benefitted greatly from the contributions of a number of senior collaborators including Ian R. Gould, Jan Verhoeven, Joshua L. Goodman, Joseph P. Dinnocenzo, Ralph H. Young, David Lee Phillips, Han Zuilhof, and Debra Egolf and postdoctoral and graduate students Frances Markel, Kristen Kulinowski, Dietrich Tittelbach-Helmrich, Jerry Godbout, Matt Pietrzykowski, Mark Lilichenko, and Mark Waterland. High school teacher Gary Heim obtained the previously unpublished resonance Raman spectra of the phenylcyclopropane/TCNE charge-transfer complex.

References and Notes

(1) Barbara, P. F.; Meyer, T. J.; Ratner, M. A. *J. Phys. Chem.* **1996**, *100*, 13148−13168.
(2) Marcus, R. A. *Rev. Mod. Phys.* **1993**, *65*, 599.
(3) Jortner, J. *J. Chem. Phys.* **1976**, *64*, 4860−4867.
(4) Newton, M.; Sutin, N. *Annu. Rev. Phys. Chem.* **1984**, *35*, 437.
(5) Newton, M. D. *Chem. Rev.* **1991**, *91*, 767−792.
(6) Marcus, R. A.; Sutin, N. *Biochim. Biophys. Acta* **1985**, *811*, 265−322.
(7) Mikkelsen, K. J.; Ratner, M. A. *Chem. Rev.* **1987**, *87*, 113−153.
(8) Kestner, N. R.; Logan, J.; Jortner, J. *J. Phys. Chem.* **1974**, *78*, 2148−2166.
(9) Myers, A. B. *Chem. Phys.* **1994**, *180*, 215−230.
(10) Marcus, R. A. *J. Phys. Chem.* **1989**, *93*, 3078−3086.
(11) Gould, I. R.; Noukakis, D.; Gomez-Jahn, L.; Young, R. H.; Goodman, J. L.; Farid, S. *Chem. Phys.* **1993**, *176*, 439−456.
(12) Myers, A. B. *J. Raman Spectrosc.* **1997**, *28*, 389−401.
(13) Myers, A. B. *Acc. Chem. Res.* **1997**, *30*, 519−527.
(14) Myers, A. B. Excited electronic state properties from ground-state resonance Raman intensities. In *Laser Techniques in Chemistry*; Myers, A. B., Rizzo, T. R., Eds.; Wiley: New York, 1995; pp 325−384.
(15) Myers, A. B.; Mathies, R. A. Resonance Raman intensities: A probe of excited-state structure and dynamics. In *Biological Applications of Raman Spectroscopy*; Spiro, T. G., Ed.; Wiley: New York, 1987; Vol. 2; pp 1−58.
(16) Myers, A. B. *Chem. Rev.* **1996**, *96*, 911−926.
(17) Doorn, S. K.; Hupp, J. T. *J. Am. Chem. Soc.* **1989**, *111*, 1142−1144.
(18) Williams, R. D.; Petrov, V. I.; Lu, H. P.; Hupp, J. T. *J. Phys. Chem. A* **1997**, *101*, 8070−8076.
(19) Meyer, T. J. *Acc. Chem. Res.* **1989**, *22*, 1048.
(20) Mirkin, C. A.; Ratner, M. A. *Annu. Rev. Phys. Chem.* **1992**, *43*, 719.
(21) Gust, D.; Moore, T. A.; Moore, A. L. *Acc. Chem. Res.* **1993**, *26*, 198.
(22) Wasielewski, M. R. *Chem. Rev.* **1992**, *92*, 435.
(23) Lax, M. *J. Chem. Phys.* **1952**, *20*, 1752−1760.
(24) Nafie, L.; Stein, P.; Fanconi, B.; Peticolas, W. L. *J. Chem. Phys.* **1970**, *52*, 1584−1588.
(25) Albrecht, A. C. *J. Chem. Phys.* **1961**, *34*, 1476−1484.
(26) Lee, S.-Y.; Heller, E. J. *J. Chem. Phys.* **1979**, *71*, 4777−4787.
(27) Heller, E. J.; Sundberg, R. L.; Tannor, D. *J. Phys. Chem.* **1982**, *86*, 1822−1833.
(28) Myers, A. B.; Mathies, R. A.; Tannor, D. J.; Heller, E. J. *J. Chem. Phys.* **1982**, *77*, 3857−3866.
(29) Tannor, D. J.; Heller, E. J. *J. Chem. Phys.* **1982**, *77*, 202.
(30) Takagahara, T.; Hanamura, E.; Kubo, R. *J. Phys. Soc. Jpn.* **1977**, *43*, 802−810.
(31) Lee, D.; Albrecht, A. C. *Adv. Infrared Raman Spectrosc.* **1985**, *12*, 179−213.
(32) Sue, J.; Yan, Y. J.; Mukamel, S. *J. Chem. Phys.* **1986**, *85*, 462−474.
(33) Watanabe, J.; Kinoshita, S.; Kushida, T. *J. Chem. Phys.* **1987**, *87*, 4471−4477.
(34) Mukamel, S. *Principles of nonlinear optical spectroscopy*; Oxford University Press: New York, 1995.
(35) Fujimura, Y.; Kono, H.; Nakajima, T.; Lin, S. H. *J. Chem. Phys.* **1981**, *75*, 99−106.
(36) Ziegler, L. D. *Acc. Chem. Res.* **1994**, *27*, 1−8.
(37) Li, B.; Johnson, A. E.; Mukamel, S.; Myers, A. B. *J. Am. Chem. Soc* **1994**, *116*, 11039−11047.
(38) Gu, Y.; Widom, A.; Champion, P. M. *J. Chem. Phys.* **1994**, *100*, 2547−2560.
(39) de Boeij, W. P.; Pshenichnikov, M. S.; Duppen, K.; Wiersma, D. A. *Chem. Phys. Lett.* **1994**, *224*, 243−252.
(40) Kirkwood, J. C.; Ulness, D. J.; Albrecht, A. C. *J. Chem. Phys.* **1998**, *108*, 9425−9435.
(41) Jensen, P. W. *Chem. Phys. Lett.* **1977**, *45*, 415−418.
(42) Smith, M. L.; McHale, J. L. *J. Phys. Chem.* **1985**, *89*, 4002−4007.
(43) Michaelian, K. H.; Rieckhoff, K. E.; Voigt, E. M. *Chem. Phys. Lett.* **1976**, *39*, 521−524.
(44) Markel, F.; Ferris, N. S.; Gould, I. R.; Myers, A. B. *J. Am. Chem. Soc.* **1992**, *114*, 6208−6219.
(45) Kulinowski, K.; Gould, I. R.; Myers, A. B. *J. Phys. Chem.* **1995**, *99*, 9017−9026.
(46) Myers, A. B. *Annu. Rev. Phys. Chem.* **1998**, *49*, 267−295.
(47) Wendt, H.; Richert, R. *J. Phys. Chem. A* **1998**, *102*, 5775−5781.
(48) Fourkas, J. T.; Benigno, A.; Berg, M. *J. Chem. Phys.* **1993**, *99*, 8552−8558.
(49) Berg, M. *Chem. Phys. Lett.* **1994**, *228*, 317−322.
(50) Berg, M. A. *J. Phys. Chem. A* **1998**, *102*, 17−30.
(51) Tran, V.; Schwartz, B. J. *J. Phys. Chem. B* **1999**, *103*, 5570−5580.
(52) Wegewijs, B.; Paddon-Row, M. N.; Braslavsky, S. E. *J. Phys. Chem. A* **1998**, *102*, 8812−8818.
(53) Su, Y.; Tripathi, G. N. R. *Chem. Phys. Lett.* **1992**, *188*, 388−394.
(54) Johnson, A. E.; Myers, A. B. *J. Phys. Chem.* **1996**, *100*, 7778−7788.
(55) Zong, Y.; McHale, J. L. *J. Chem. Phys.* **1997**, *106*, 4963−4972.
(56) Zong, Y.; McHale, J. L. *J. Chem. Phys.* **1997**, *107*, 2920−2929.
(57) Cao, X.; McHale, J. L. *J. Chem. Phys.* **1998**, *109*, 1901−1911.
(58) Kulinowski, K.; Gould, I. R.; Ferris, N. S.; Myers, A. B. *J. Phys. Chem.* **1995**, *99*, 17715−17723.
(59) Wynne, K.; Galli, C.; Hochstrasser, R. M. *J. Chem. Phys.* **1994**, *100*, 4797−4810.
(60) Kimura, Y.; Takebayashi, Y.; Hirota, N. *J. Chem. Phys.* **1998**, *108*, 1485−1498.
(61) Rubtsov, I. V.; Yoshihara, K. *J. Phys. Chem.* **1997**, *101*, 6138.
(62) Hush, N. S. *Prog. Inorg. Chem.* **1967**, *8*, 391.
(63) Cave, R. J.; Newton, M. D. *J. Chem. Phys.* **1997**, *106*, 9213−9226.
(64) Strickler, S. J.; Berg, R. A. *J. Chem. Phys.* **1962**, *37*, 814.
(65) Gould, I. R.; Farid, S. *J. Am. Chem. Soc.* **1988**, *110*, 7883−7885.
(66) Dresner, J.; Prochorow, J.; Sobolewski, A. *Chem. Phys. Lett.* **1978**, *54*, 292−294.
(67) Doolen, R.; Simon, J. D.; Baldridge, K. K. *J. Phys. Chem.* **1995**, *99*, 13938−13947.
(68) Okajima, S.; Lim, B. T.; Lim, E. C. *J. Chem. Phys.* **1980**, *73*, 3512−3514.
(69) Mortensen, O. S.; Siebrand, W.; Tarr, A. W. *Chem. Phys.* **1988**, *125*, 231−245.
(70) Siebrand, W.; Williams, D. F. *J. Chem. Phys.* **1968**, *49*, 1860−1871.

(71) Britt, B. M.; McHale, J. L.; Friedrich, D. M. *J. Phys. Chem.* **1995**, *99*, 6347−6355.
(72) Frey, J. E.; Andrews, A. M.; Ankoviac, D. G.; Beaman, D. N.; Du Pont, L. E.; Elsner, T. E.; Lang, S. R.; Oosterbaan Zwart, M. A.; Seagle, R. E.; Torreano, L. A. *J. Org. Chem.* **1990**, *55*, 606−624.
(73) Rossi, M.; Buser, U.; Haselbach, E. *Helv. Chim. Acta* **1976**, *59*, 1039−1053.
(74) Frey, J. E.; Cole, R. D.; Kitchen, E. C.; Suprenant, L. M.; Sylwestrzak, M. S. *J. Am. Chem. Soc.* **1985**, *107*, 748−755.
(75) Kumble, R.; Rush, T. S., III; Blackwood, M. E., Jr.; Kozlowski, P. M.; Spiro, T. G. *J. Phys. Chem. B* **1998**, *102*, 7280−7286.
(76) Phillips, D. L.; Myers, A. B. *J. Chem. Phys.* **1991**, *95*, 226−243.
(77) Britt, B. M.; McHale, J. L. *Chem. Phys. Lett.* **1997**, *270*, 551−556.
(78) Hayashi, M.; Yang, T.-S.; Yu, J.; Mebel, A.; Lin, S. H. *J. Phys. Chem. A* **1997**, *101*, 4156−4162.
(79) Hayashi, M.; Yang, T.-S.; Yu, J.; Mebel, A.; Chang, R.; Lin, S. H.; Rubtsov, I. V.; Yoshihara, K. *J. Phys. Chem. A* **1998**, *102*, 4256−4265.
(80) Juanós i Timoneda, J.; Peters, K. S. *J. Phys. Chem.* **1996**, *100*, 16864−16873.
(81) Dixon, D. A.; Miller, J. S. *J. Am. Chem. Soc.* **1987**, *109*, 3656−3664.
(82) Lilichenko, M.; Tittelbach-Helmrich, D.; Verhoeven, J. W.; Gould, I. R.; Myers, A. B. *J. Chem. Phys.* **1998**, *109*, 10958−10969.
(83) In ref 82, an error was made in the conversion from dimensionless displacements to bond length and bond angle changes. The values quoted in this paper are the correct ones. See the following erratum: Lilichenko, M.; Kelley, A. M. *J. Chem. Phys.* **1999**, *111*, 2345−2346.
(84) Dockery, K. P.; Dinnocenzo, J. P.; Farid, S.; Goodman, J. L.; Gould, I. R.; Todd, W. P. *J. Am. Chem. Soc.* **1997**, *119*, 1876−1883.
(85) Dinnocenzo, J. P.; Simpson, T. R.; Zuilhof, H.; Todd, W. P.; Heinrich, T. *J. Am. Chem. Soc.* **1997**, *119*, 987−993.
(86) Dinnocenzo, J. P.; Zuilhof, H.; Lieberman, D. R.; Simpson, T. R.; McKechney, M. W. *J. Am. Chem. Soc.* **1997**, *119*, 994−1004.
(87) Godbout, J. T.; Pietrzykowski, M. D.; Gould, I. R.; Goodman, J. L.; Kelley, A. M. *J. Phys. Chem. A* **1999**, *103*, 3876−3883.
(88) Godbout, J. T.; Zuilhof, H.; Gould, I. R.; Goodman, J. L.; Dinnocenzo, J. P.; Kelley, A. M. *J. Raman Spectrosc.*, submitted.
(89) Borsenberger, P. M.; Weiss, D. S. In *Organic photoreceptors for imaging systems*; Marcel Dekker: New York, 1998.
(90) Bässler, H. *Phys. Status Solidi* **1993**, *175*, 15.
(91) Young, R. H. *Philos. Mag. B* **1994**, *69*, 577−594.
(92) Gartstein, Y. N.; Conwell, E. M. *Chem. Phys. Lett.* **1994**, *217*, 41−47.
(93) Soos, Z. G.; Schmidt, S. J. *Chem. Phys. Lett.* **1997**, *265*, 427−433.
(94) Novikov, S. V.; Dunlap, D. H.; Kenkre, V. M.; Parris, P. E.; Vannikov, A. V. *Phys. Rev. Lett.* **1998**, *81*, 4472−4475.
(95) Mort, J.; Pfister, G.; Grammatica, S. *Solid State Commun.* **1976**, *18*, 693−696.
(96) Santos Lemus, S. J.; Hirsch, J. *Philos. Mag. B* **1986**, *53*, 25−39.
(97) Lee, S. Y.; Boo, B. H. *J. Phys. Chem.* **1996**, *100*, 15073−15078.
(98) Egolf, D.; Waterland, M. R.; Kelley, A. M. *J. Am. Chem. Soc.*, submitted.
(99) Closs, G. L.; Miller, J. R. *Science* **1988**, *240*, 440−447.
(100) Oevering, H.; Verhoeven, J. W.; Paddon-Row: M. N.; Warman, J. M. *Tetrahedron* **1989**, *45*, 4751−4766.
(101) Pullen, S. H.; Edington, M. D.; Studer-Martinez, S. L.; Simon, J. D.; Staab, H. A. *J. Phys. Chem. A* **1999**, *103*, 2740−2743.
(102) Marder, S. R.; Cheng, L.-T.; Tiemann, B. G.; Friedli, A. C.; Blanchard-Desce, M.; Perry, J. W.; Skindhøj, J. *Science* **1994**, *263*, 511−514.
(103) Bublitz, G. U.; Ortiz, R.; Runser, C.; Fort, A.; Barzoukas, M.; Marder, S. R.; Boxer, S. G. *J. Am. Chem. Soc.* **1997**, *119*, 2311−2312.
(104) Blanchard-Desce, M.; Wortmann, R.; Lebus, S.; Lehn, J.-M.; Krämer, P. *Chem. Phys. Lett.* **1995**, *243*, 526−532.
(105) Dekkers, A. W. J. D.; Verhoeven, J. W.; Speckamp, W. N. *Tetrahedron* **1973**, *29*, 1691−1696.
(106) Phillips, D. L.; Gould, I. R.; Verhoeven, J. W.; Tittelbach-Helmrich, D.; Myers, A. B. *Chem. Phys. Lett.* **1996**, *258*, 87−93.
(107) Lilichenko, M.; Verhoeven, J. W.; Myers, A. B. *Spectrochim. Acta A* **1997**, *53*, 2079−2093.
(108) Zwier, J. M.; Wiering, P. G.; Brouwer, A. M.; Bebelaar, D.; Buma, W. J. *J. Am. Chem. Soc.* **1997**, *119*, 11523−11533.
(109) Wynne, K.; Reid, G. D.; Hochstrasser, R. M. *J. Chem. Phys.* **1996**, *105*, 2287−2297.
(110) Arnett, D. C.; Vöhringer, P.; Scherer, N. F. *J. Am. Chem. Soc.* **1995**, *117*, 12262−12272.
(111) Reid, P. J.; Silva, C.; Barbara, P. F.; Karki, L.; Hupp, J. T. *J. Phys. Chem.* **1995**, *99*, 2609−2616.
(112) Johnson, A. E.; Myers, A. B. *J. Chem. Phys.* **1996**, *104*, 2497−2507.